Journal of the Mechanics and Physics of Solids 64 (2014) 184–197

Contents lists available at ScienceDirect

Journal of the Mechanics and Physics of Solids

journal homepage: www.elsevier.com/locate/jmps

Damage–breakage rheology model and solid-granular transition near brittle instability

Vladimir Lyakhovsky [a,*], Yehuda Ben-Zion [b]

[a] Geological Survey of Israel, Jerusalem 95501, Israel
[b] Department of Earth Sciences, University of Southern California, Los Angeles, CA 90089-0740, USA

ARTICLE INFO

Article history:
Received 21 September 2012
Received in revised form
15 September 2013
Accepted 10 November 2013
Available online 26 November 2013

Keywords:
Fracture
Phase transformation
Dynamics
Rock
Granular material
Constitutive behavior

ABSTRACT

We develop a continuum-based theoretical framework that describes brittle instability and localization of deformation into a narrow slip zone as a phase transition between damaged solid and granular material. The formulation is based on irreversible thermodynamics of damage and breakage processes, each associated with a single key state variable, and corresponding energy functions for the damaged solid and granular material. Dynamic instability is associated with a critical level of damage in the solid, leading to loss of convexity of the solid energy function and transition to a granular phase associated with lower energy level. Depending on the confining stress and other conditions, the failure process in the generated granular phase may be associated with mode I and fragmentation or mode II and granular flow. The developed model provides a new approach for analyzing in a unified way various aspects of brittle failure and localization of deformation, with evolving elastic moduli, evolving slip rates and evolving material phases. Numerical simulations indicate that the key parameters governing the evolution from a slow failure process to dynamic slip, and the related transition from damaged solid to granular material, can be constrained by laboratory and seismological observations.

1. Introduction

Rocks, ceramics and similar materials, under relatively low pressure and temperature and without a pre-existing large failure zone, respond to differential stress beyond the elastic limit by generation of distributed brittle cracking (damage) in the bulk. The gradual distributed cracking is manifested macroscopically by changes of average elastic properties and related phenomena such as reduction of wave speeds. This process is observed in numerous laboratory fracturing experiments (e.g., Jaeger and Cook, 1979; Lockner et al., 1992; Stanchits et al., 2006) and it can be modeled effectively by various damage rheology frameworks (e.g. Hamiel et al. 2004, 2009; Bhat et al., 2011). When the level of damage reaches a critical value, the material sustains macroscopic brittle instability involving dynamic rupture and localization of deformation. The volume with intense damage around the localized rupture tip is referred to as the process region or zone (e.g., Broberg, 1999). The motion of the process region leaves behind a zone of localized brittle deformation with granulated material that is referred to as the slip zone (e.g. Ben-Zion and Sammis, 2003, and references therein). Various observational and theoretical results suggest that the discussed brittle failure process is associated with a phase transition from a damaged solid prior to localization to a granular phase of material within the generated slip zone (Ben-Zion, 2008, Section 7).

* Corresponding author.
E-mail addresses: vladi@gsi.gov.il, vladi@geos.gsi.gov.il (V. Lyakhovsky), benzion@usc.edu (Y. Ben-Zion).

0022-5096/$ - see front matter © 2013 Elsevier Ltd. All rights reserved.
http://dx.doi.org/10.1016/j.jmps.2013.11.007

Initial quantitative results on aspects of the solid-granular transition and related dynamic phenomena are given by Lyakhovsky et al. (2011) using a continuum viscoelastic damage model and Ben-Zion et al. (2011) based on a statistical physics framework. The goal of this paper is to provide a more complete quantitative description of the transition from a stable damaged solid to unstable material that includes a granulated slip zone. The developments are done within the continuum damage model of Lyakhovsky et al. (1997), (2011), augmented by results from a continuum breakage mechanics (Einav, 2007a,b). The developed continuum damage–breakage model accounts for the density of distributed cracking and other internal flaws in damaged solid rocks with a scalar damage parameter, and addresses the grain size distribution of a fluid- or gas-like granular phase with a breakage parameter. The model provides a framework that can be used to analyze the progression of deformation from a stable distributed brittle failure in a solid with evolving elastic moduli, to localization and dynamic rupture in a zone with one or more vanishing elastic moduli. This generalizes related transitions from slow deformation to dynamic rupture on a frictional interface where the process is limited to a surface (e.g., Rice, 1980, 1993), and in volumes governed by plastic with unchanged elastic moduli rheology (e.g., Rudnicki and Rice, 1975; Perrin and Leblond, 1993).

When the damage reaches at a certain region a critical value leading to dynamic instability, the generated failure zone can be associated with a pseudo-liquid or a pseudo-gas granular phase. Under confinement, a pseudo-liquid granular phase is produced and subsequent failure is associated with shear granular flow. With little or no confinement, a pseudo-gas phase is generated and subsequent failure is associated with expanding fragmentation process. Numerical simulations illustrate several aspects of the developed continuum damage–breakage model. A theoretical treatment of the reversed transition from granulated material to damaged solid will be provided in a follow up work.

2. Theory

2.1. General thermodynamic formulation

To describe a solid-granular transition we combine aspects of two formulations: Continuum Damage Mechanics (CDM) and Continuum Breakage Mechanics (CBM). Both are based on irreversible thermodynamics and each introduces an additional state variable: damage parameter $\alpha=[0{:}1]$ in the CDM and breakage parameter $B=[0{:}1]$ in the CBM. The damage parameter of the CDM (e.g., Kachanov, 1986; Rabotnov, 1988; Krajcinovic, 1996; Lemaitre, 1996; Allix and Hild, 2002) connects the evolution of elastic moduli with changes of crack density through a non-dimensional intensive variable characterizing material volumes large enough to allow smooth description of the distribution of internal flaws (e.g., micro-cracks in laboratory specimen). The breakage parameter of the CBM (Einav, 2007a,b) measures the relative distance of the current grain size distribution of a granular material between the initial and ultimate states. The free energy, F_S, of a damaged solid with distributed cracking has additional terms to those characterizing reversible elastic materials (e.g., Lyakhovsky et al., 1997, 2011). The free energy, F_B, of the CBM is assumed to be a linear function of the breakage parameter (Einav, 2007a,b). Following these ideas we write the total free energy of the Continuum Damage–Breakage Mechanics (CDBM) model as a linear superposition of F_S characterizing the solid phase and F_B of the granular phase:

$$F(T,\ \varepsilon_{ij},\ \alpha,\ B) = (1-B)\cdot F_S(T,\ \varepsilon_{ij},\ \alpha) + B\cdot F_B(T,\ \varepsilon_{ij}). \tag{1}$$

Here T is the temperature and $\varepsilon_{ij}=\varepsilon_{ij}^{(t)}-\varepsilon_{ij}^{(p)}$ is the elastic strain tensor given by the difference between the total and permanent irreversible deformation. As mentioned, α and B are the damage and breakage variables, respectively. The linear superposition of the solid and granular energy terms (1) preserves the linear dependence of the total energy on the breakage parameter, and assures the convexity of the total energy if one or both F_S and F_B are convex and B varies between zero and one. According to the general idea of Maxwell visco-elastic rheology, the energy function of the system depends only on the difference between the total and irreversible strain components rather than having explicit connections to both (e.g., Malvern, 1969). The irreversible strain accumulation may be neglected for the solid phase, but it becomes essential for the post-failure flow of the granular phase. Details of the energy form, kinetics of the evolving damage ($d\alpha/dt$) and breakage (dB/dt) parameters, as well as relations controlling the rate of irreversible strain accumulation ($d\varepsilon_{ij}^{(p)}/dt$), are discussed in the following sections.

2.2. Free energy of the solid phase

For the solid phase we use the energy form previously discussed in Lyakhovsky et al. (1997) and Hamiel et al. (2011), incorporating two Hookean quadratic terms and a third term that couples volumetric and shear strain:

$$F_S(\varepsilon_{ij},\alpha) = \frac{1}{\rho}\left(\frac{\lambda}{2}I_1^2+\mu I_2-\gamma I_1\sqrt{I_2}\right) \tag{2}$$

where λ and μ are Lame constants, $I_1=\varepsilon_{ij}\delta_{ij}$ and $I_2=\varepsilon_{ij}\varepsilon_{ij}$ are the first and second invariants of the strain tensor ε_{ij}, and γ is an additional modulus of a damaged solid.

Taking the derivative of the energy form (2) with respect to the strain leads (Eq. (A11) of the Appendix) to the following stress-strain relation:

$$\sigma_{ij} = (\lambda - \gamma/\xi) I_1 \delta_{ij} + (2\mu - \gamma\xi)\varepsilon_{ij}. \tag{3}$$

The effective elastic moduli in (3) are functions of the strain invariants ratio, $\xi = I_1/\sqrt{I_2}$, which characterizes various states of loading. Its value varies between $\xi = -\sqrt{3}$ for 3-D compaction to $\xi = +\sqrt{3}$ for 3-D expansion; $\xi = \pm 1$ correspond to tension and compression, while $\xi = 0$ corresponds to zero volumetric strain. The specific detailed relation between the energy (2) and the damage state variable is established by making the elastic moduli functions of α. Given the available experimental constraints, Agnon and Lyakhovsky (1995) assumed that the moduli μ and γ are linear functions of α and that λ is constant. Hamiel et al. (2004) reviewed this assumption and demonstrated that a power-law relation $\gamma(\alpha)$ improves the quality of fitting stress-strain curves observed in laboratory fracture experiments with model predictions. The same power-law relation also leads to a transition between stable and unstable damage evolution in rocks (Hamiel et al., 2004). For mathematical simplicity we adopt here the linear relations:

$$\begin{aligned} &\lambda = \lambda_0, \\ &\mu = \mu_0 + \alpha\xi_0\gamma_r, \\ &\gamma = \alpha\gamma_r, \end{aligned} \tag{4}$$

where λ_0, μ_0 and $\gamma = 0$ are the elastic moduli of a damage-free material ($\alpha = 0$), and $\lambda = \lambda_0$, $\mu = \mu_0 + \xi_0\gamma_r$ and $\gamma = \gamma_r$ give the moduli values at maximum damage level ($\alpha = 1$). The parameter ξ_0 is a critical value of the strain invariants ratio ($\xi = I_1/\sqrt{I_2}$) at the onset of damage accumulation and is connected to the internal friction angle of the Byerlee (1978) friction law for rocks (Agnon and Lyakhovsky, 1995). During damage accumulation the modulus γ increases and the shear modulus μ decreases. This leads (Fig. 1) to material evolution from linear elastic solid ($\alpha = 0$) to strongly non-linear behavior and macroscopic brittle instability at a critical damage level (α_c).

Two mathematically different conditions can be utilized for analyzing the macroscopic stability condition for material in a solid state ($B = 0$) below the critical damage level $\alpha < \alpha_{cr}$. The first is convexity of the elastic strain energy, which is necessary for the existence of a unique solution of the static problem (e.g., Ekeland and Temam, 1976). The second is a change of the elasto-dynamic equation to ellipticity (e.g., Rudnicki and Rice, 1975). These two conditions are not always identical, especially for non-linear elasticity. For the energy form (2), the convexity condition is stronger and is achieved prior to the transition to ellipticity (Lyakhovsky et al., 2011). Starting with the classical *van der Waals* theory, non-convex energy functions were used commonly in different theoretical models of multi-phase systems (e.g., Ericksen, 1998). Mathematically, the convexity condition implies positivity of all the eigenvalues of the Hessian matrix ($\partial^2 F_S/\partial\varepsilon_{ij}\partial\varepsilon_{kl}$), which can be expressed by the following inequalities (Lyakhovsky et al., 2011):

$$(2\mu - \gamma\xi)^2 + (2\mu - \gamma\xi)(3\lambda - \gamma\xi) + (\lambda\gamma\xi - \gamma^2)(3 - \xi^2) > 0, \tag{5a}$$

$$2\mu - \gamma\xi > 0. \tag{6a}$$

Within the interval of the strain invariants ratio $-\sqrt{3} \le \xi \le \xi_0$, corresponding to loading from 3-D compaction with gradually increased deviatoric stress until the onset of fracturing, both conditions ((5a), (6a)) are satisfied for $\alpha < 1$. With

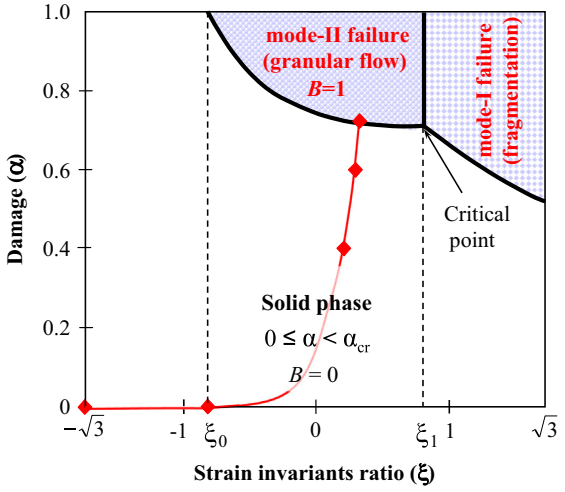

Fig. 1. Schematic diagram illustrating the critical level of damage versus the strain invariants ratio ($\xi = I_1/\sqrt{I_2}$) for $\lambda_0 = \mu_0$. Solid black lines separate regions where different phases exist and correspond to convexity loss of the solid energy function. The parameter ξ_0 prescribes the onset of damage accumulation. The material is stable for $\xi < \xi_0$. The parameter ξ_1 defines the location of the critical point where all three phases, solid, pseudo-liquid and pseudo-gas exist for $\alpha = \alpha_{cr}$. Red line with markers represents a loading path leading to a solid-granular transition (see Fig. 4). (For interpretation of the references to color in this figure legend, the reader is referred to the web version of this article.)

further increase of the deviatoric stress, the damage increases toward its critical value ($\alpha=\alpha_{cr}$) and condition (5a) is violated first. This occurs within the interval of the strain invariants ratio up to a certain value ξ_1 ($\xi_0 \le \xi \le \xi_1$). This type of loss of convexity is associated with mode-II failure and transition to a granular flow under compression (Fig. 1). The granular material under these conditions may be referred to as pseudo-liquid. At higher values of the strain invariants ratio ($\xi_1 < \xi$), condition (6a) is violated first at $\alpha=\alpha_{cr}$. In this case at least one of the principal stress values becomes tensile and there is mode-I failure that leads to fragmentation (Fig. 1). In this case the granular material may be referred to as pseudo-gas.

At the transition between mode-I and mode-II failures associated with the point $\alpha=\alpha_{cr}$ and $\xi=\xi_1$, all eigen values of the Hessian matrix vanish simultaneously and conditions ((5a), (6a)) are reduced to:

$$\lambda-\gamma/\xi=0, \tag{5b}$$

$$2\mu-\gamma\xi=0. \tag{6b}$$

Combining (4) with ((5b), (6b)) leads to a solution for the values of α_{cr} and ξ_1:

$$\xi_1=\xi_0+\sqrt{\xi_0^2+2\frac{\mu_0}{\lambda_0}}, \tag{7}$$

$$\alpha_1=\alpha_{cr}(\xi_1)=\frac{\lambda_0\xi_1}{\gamma_r}. \tag{8}$$

A comparison of ((5b), (6b)) with the stress-strain relation (3) indicates that all eigen values of the Hessian matrix vanish simultaneously when both effective elastic moduli of the damaged solid are zero. This resembles the mathematical definition of the critical (triple) point of a classical thermodynamic system. For a pure substances (say liquid or gas), there is an inflection point in the critical isotherm (constant temperature line) on a P–V diagram, where both the first and second partial derivatives of the pressure with respect to the volume at constant temperature are zero.

2.3. Free energy of the granular phase

The constitutive relations for cohesionless granular material should account for vanishing tensile modulus while the compressive modulus remains finite (e.g., Nguyen et. al., 2003, Karrech et. al., 2007). Based on this, Myasnikov and Oleinikov (1991) discussed a mathematical model for granular material as a limit case of isotropic visco-elastic or elasto-plastic media that respond differently to tension and compression using the energy form (2). See also Ben-Zion (2008, Section 7). Since the energy, F_B, of the CBM is assumed to be a linear function of the breakage parameter (Einav, 2007a,b), and the strain energy function does not depend on the damage value which is relevant for the solid phase only, we write the energy of the granular material as:

$$F_B(\varepsilon_{ij})=\frac{1}{\rho}\left(\frac{\lambda_B}{2}I_1^2+\mu_B I_2-\gamma_B I_1\sqrt{I_2}\right), \tag{9}$$

with three constant elastic moduli. The transition between the pseudo-liquid (granular flow) and pseudo-gas (fragmentation) phases is associated with loss of convexity of F_B represented by a vertical line in the (ξ, α) space (Fig. 1). Since all three phases, solid, pseudo-liquid and pseudo-gas, co-exist in the triple (critical) point (ξ_1, α_1), all eigen values of the Hessian matrix associated with F_B should be equal zero at this point. These conditions are satisfied if the elastic moduli in (9) are proportional, with some coefficient θ, to the values of the elastic moduli of the solid phase (4) at the damage level $\alpha=\alpha_1$

$$\begin{aligned}&\lambda_B=\theta\lambda(\alpha_1)=\theta\lambda_0\\&\mu_B=\theta\mu(\alpha_1)=\theta(\mu_0+\alpha_1\xi_0\gamma_r)\\&\gamma_B=\theta\gamma(\alpha_1)=\theta\alpha_1\gamma_r\end{aligned} \tag{10}$$

Fig. 2 shows normalized energy values (F_S/I_2, $\lambda_0=\mu_0=1$) for the solid phase (black line) and (F_B/I_2) for the granular phase (red lines) for $\alpha=\alpha_{cr}(\xi)$, within the interval $\xi_0<\xi<\xi_1$ where a transition from solid to granular pseudo-liquid phase is expected. The energy of the granular phase is always below that of the solid phase for $\theta<1$, providing a proper energetic transition from higher energy solid state to lower energy granular phase. The θ value controls the amount of energy released during the transition from solid to granular phase. This energy release is equivalent to the latent heat of phase transitions in classical thermodynamics. The condition $F_S>F_B$ prohibits in the absence of material healing the reversed transition from granular to solid, even under compressive stresses without any differential load. In the present paper we focus on the solid-granular transition. An extension of the formulation with healing of the breakage parameter that may be used to analyze the granular-solid transition will be addressed in the discussion and developed in a follow up paper.

2.4. Instantaneous transition from solid to granular phase

In this section we discuss some general features of the solid-granular transition, assuming infinitely fast kinetic of the breakage evolution that leads to instantaneous transition when the solid becomes unstable. The kinetics of the damage–breakage process will be discussed in the next section.

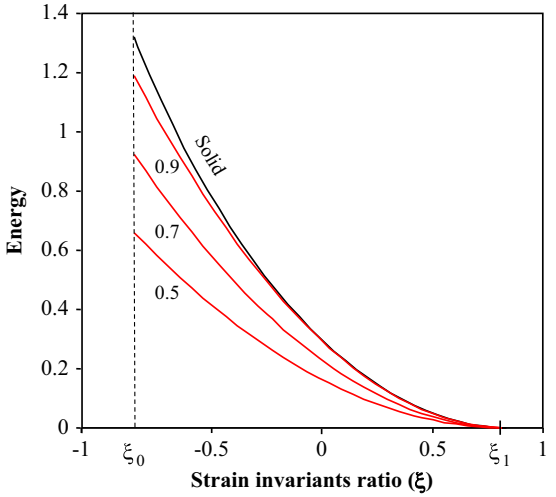

Fig. 2. Normalized energy (F_S/I_2, $\lambda_0=\mu_0=1$) of the solid phase (black line) and granular phase (F_B/I_2) within the interval (red lines) $\xi_0<\xi<\xi_1$ and $\alpha=\alpha_{cr}(\xi)$ where a transition from solid to granular pseudo-liquid phase is expected. The energy for the granular phase is shown for $\theta=0.9$, 0.7 and 0.5. See text for additional explanation. (For interpretation of the references to color in this figure legend, the reader is referred to the web version of this article.)

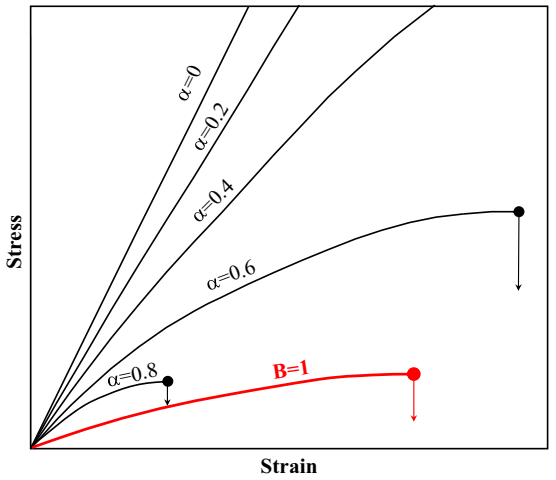

Fig. 3. Schematic stress–strain diagrams (not on scale) under a loading path starting with 3-D compaction ($\xi=-\sqrt{3}$) and going toward 3-D extension ($\xi=\sqrt{3}$) for different damage values $\alpha=0$, 0.2, 0.4, 0.6, and 0.8 (black lines). The red line represents the stress-strain curve for the granular phase ($B=1$). (For interpretation of the references to color in this figure legend, the reader is referred to the web version of this article.)

Fig. 3 shows schematic stress-strain diagrams (not on scale) under a loading path starting with 3-D compaction ($\xi=-\sqrt{3}$) and going toward 3-D extension ($\xi=\sqrt{3}$). Fixed value of the damage parameter ($\alpha=$Const.) is assumed for the entire loading path. This process could only be realized in laboratory experiments or natural conditions if the rate of damage accumulation is well below the loading rate and there is not enough time for α to evolve. In the (ξ, α) space (Fig. 1) such loading path with a constant α value is represented by a straight horizontal line starting at the left edge and going to the right. For small α-values ($\alpha=0$, 0.2, and 0.4) the solid state is stable through the whole loading path and transition to another phase is not expected. For an elevated damage value $\alpha=0.6$, the loading path crosses the line separating the solid and pseudo-gas phase at $\xi>\xi_1$ where fragmentation occurs. The effective elastic modulus vanishes and the solid becomes unstable (Fig. 3). The fragmented material cannot support any deviatoric stress and further behavior should be described in terms of pressure and volumetric expansion. Here we are interested primarily in the transition from damaged solid to granular flow. With high damage values ($\alpha=0.8$), the solid material becomes unstable for horizontal loading path in the (ξ, α) space at an earlier stage $\xi<\xi_1$ (compare the lines for $\alpha=0.6$ and 0.8 in Fig. 3). However, this loading path meets a transition to the pseudo-liquid granular phase (Fig. 1), which involves stable granular flow at the transition (red line in Fig. 3). Rapid change from $B=0$ for solid state to $B=1$ for granular state is associated with a stress drop, and the stress-strain path jumps (Fig. 3) from the black line (solid phase) to the red one (pseudo-liquid phase). Further loading can take place along the red line. If the loading rate is faster than stress relaxation due to granular flow, evolution of elastic strain toward 3-D extension may bring the system to fragmentation terminating the loading path of the granular phase.

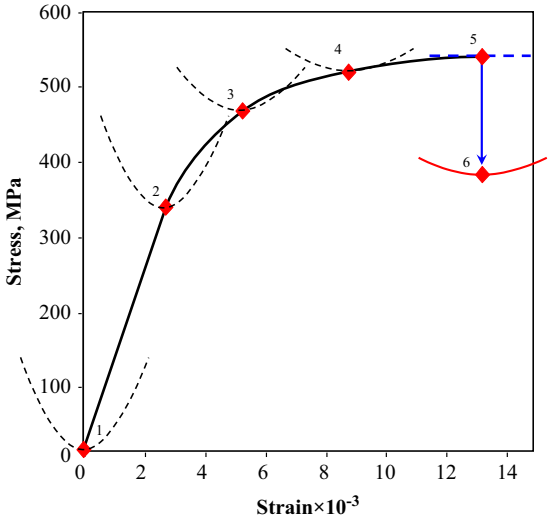

Fig. 4. Stress–strain diagrams under the loading path shown in Fig. 1. The dashed lines illustrate the elastic energy change under small perturbation around stable states (markers 1 to 4) of the solid phase. The flattening of the parabolas (markers 3 and 4) represents material degradation due to damage increase compared with the damage free material (markers 1 and 2). At the critical damage level ($\alpha=\alpha_{cr}$) the energy curve loses convexity (marker 5) leading to a transition to a granular phase with lower convex energy (maker 6).

A more realistic loading path with evolving damage is represented by the red line with markers in Fig. 1 and the corresponding stress-strain path in Fig. 4. The shown loading path corresponds approximately to the fracturing experiment G3 of Lockner et al. (1992), with uniaxial loading of a Westerly granite sample under 50 MPa confining pressure. The loading path starts with a 3-D compaction $\xi=-\sqrt{3}$ and $\alpha=0$ (first marker in Figs. 1 and 4). In the second marker, there is onset of damage accumulation. The stress-strain curve between the first and second markers is a straight line corresponding to linear elasticity. With progressive damage accumulation the material weakens and the stress-strain curve significantly deviates from a straight line (markers 3 and 4). The loading path is terminated when α reaches its critical value leading to a transition to granular flow. This transition is associated with a stress drop illustrated in Fig. 4 with the jump between markers 5 and 6. The magnitude of this stress drop is controlled by the θ value introduced in (10).

The evolution of the strain energy due to small perturbations around stable solutions is schematically shown in Fig. 4 by small parabolas around the markers. Since we consider small perturbations around a certain state of stress (associated mathematically with a Taylor expansion of the energy function), the energy is parabolic. For markers 1 and 2 associated with linear elasticity, the parabolas are almost the same except a shift to the new energy level. With increasing damage the effective elastic moduli decrease leading to reduced convexity of the energy function (markers 3 and 4). At the critical damage value, the energy of the damaged solid losses convexity (blue line around marker 5) and a static solution for the solid phase does not exist anymore. However, under the same strain conditions the energy of the pseudo-liquid granular phase is below the energy of the solid phase and is stable (red parabola near marker 6). As in classical phase transition theory, the system jumps from the unstable damaged solid state with higher energy to the stable granular state with lower energy.

2.5. Kinetics of the solid-granular transition

We now discuss how to describe a gradual evolution of the breakage parameter B when the solid phase becomes unstable. The entropy production, Γ_{DB}, associated with two evolving scalar state variables, damage and breakage (Eq. (A8) of the Appendix) is:

$$\Gamma_{DB}=-\frac{1}{T}\left(\frac{\partial F}{\partial \alpha}\frac{d\alpha}{dt}+\frac{\partial F}{\partial B}\frac{dB}{dt}\right). \tag{11}$$

Adopting Onsager (1931) reciprocal relations between thermodynamic forces and fluxes, we write phenomenological equations for the kinetics of the state variables α and B as a set of two coupled differential equations:

$$\begin{aligned}\frac{dB}{dt}&=C_{BB}\frac{\partial F}{\partial B}+C_{B\alpha}\frac{\partial F}{\partial \alpha}.\\ \frac{d\alpha}{dt}&=C_{\alpha B}\frac{\partial F}{\partial B}+C_{\alpha\alpha}\frac{\partial F}{\partial \alpha}\end{aligned} \tag{12}$$

The kinetic coefficients (or functions), C_{BB}, $C_{B\alpha}$, $C_{\alpha B}$, and $C_{\alpha\alpha}$, connect the thermodynamic forces associated with certain state variable with thermodynamic fluxes. The diagonal terms with C_{BB} and $C_{\alpha\alpha}$ are associated with a given state variable,

while the off-diagonal terms with $C_{\alpha B}$ and $C_{B\alpha}$ provide coupling between evolving damage with breakage and vise versa. Using Eqs. (1), (2), (4) and (10), the partial derivatives of the energy with respect to α and B are:

$$\frac{\partial F}{\partial B} = F_B - F_S$$
$$\frac{\partial F}{\partial \alpha} = -\frac{1-B}{\rho}\gamma_r I_2(\xi-\xi_0). \tag{13}$$

Substituting (13) into (12) and then into (11) we get the entropy production, Γ_{DB}, and write the condition for its non-negativity:

$$\Gamma_{DB} = \frac{1}{T}\left\{-C_{\alpha\alpha}\left[\frac{1-B}{\rho}\gamma_r I_2(\xi-\xi_0)\right]^2 - C_{BB}(F_B-F_S)^2 + +(C_{\alpha B}+C_{B\alpha})(F_B-F_S)\left[\frac{1-B}{\rho}\gamma_r I_2(\xi-\xi_0)\right]\right\} \geq 0. \tag{14}$$

The kinetic coefficients (or functions) $C_{\alpha\alpha}$ and C_{BB}, associated with quadratic terms and minus sign, should always be negative to ensure non-negative entropy production. The kinetic coefficients are often assumed to be anti-symmetric, $C_{B\alpha} = -C_{\alpha B}$, for many practical applications (e.g., deGroot and Mazur, 1962; Malvern, 1969). This would eliminates the third term in the entropy production (14) and provide its unconditional positivity. Here we suppose that accumulating damage toward the critical value leads to significant increase in the breakage parameter, while breakage processes in the solid state have small impact on the evolving damage. Therefore, we assume $C_{\alpha B}=0$ as a reasonable approximation. The energy F_B is defined to be less than F_S, so the third term in (14) is always positive if $C_{B\alpha} < 0$ when $\xi > \xi_0$. This means that damage increase ($\xi > \xi_0$) leads to increase of the breakage. The difference $F_B - F_S$ decreases with increasing ξ and becomes zero for $\xi = \xi_1$ (Fig. 2). Therefore the second term with $C_{B\alpha}$ in Eq. (12) for the breakage growth is dominant, and the first term with C_{BB} may be neglected. The resulting simplified coupled equations for the damage and breakage increase are:

$$\frac{d\alpha}{dt} = C_d(1-B)I_2(\xi-\xi_0), \quad for\ \xi \geq \xi_0 \tag{15}$$

$$\frac{dB}{dt} = C_B P(\alpha)\cdot(1-B)I_2(\xi-\xi_0), \quad for\ \xi \geq \xi_0 \tag{16}$$

where C_d and C_B are two positive kinetic constants. The rate of damage recovery for $\xi < \xi_0$ and possible breakage decrease is not considered at this stage.

Lyakhovsky et al. (2011) suggested that the probability P that a material element of a mixed solid-granular zone (mushy region) near the critical state $\alpha = \alpha_{cr}(\xi)$ is in a granular phase has a functional form

$$P(\alpha) = \frac{1}{\exp((\alpha_{cr}(\xi)-\alpha)/\beta)+1}, \tag{17}$$

where the β-value defines the width of the transitional region. For $\beta \to 0$, $P(\alpha)$ approaches the Heaviside (step) function that abruptly changes its value from zero to one. Together with fast kinetics of the breakage growth ($C_B \to \infty$), the transition from the solid to granular phase is in this case instantaneous without any mushy region. With finite values of β and C_B, accumulating damage toward the critical value leads to significant increase in the breakage value. As mentioned, we assume that breakage processes in the solid state have minor impact on the evolving damage. These results provide general guidelines for describing the deformation processes near the unstable regime $\alpha \to \alpha_{cr}(\xi)$.

2.6. Flow of the pseudo-liquid granular phase

The energy dissipation during mechanical work, Γ_M, (A6), or stress power expressed by the volume integral of the stress tensor, σ_{ij}, multiplied by the rate of irreversible strain accumulation, e^p_{ij} ($\int_V \sigma_{ij} e^p_{ij} dV$) may be neglected for the solid phase. However, accounting for energy dissipation is crucial for proper description of visco-elastic or elasto-plastic flow of the granular phase. Onsager (1931) reciprocal relations predict that the strain rate is proportional to the stress, as in the Newtonian-type viscosity. More complicate flow rules may be derived using dissipative potential and yield conditions. Starting with the pioneering works by von Mises and von Karman, several models involving yield conditions and flow rules attempted to account for the observed phenomenology of granular material (e.g., Jaeger et al., 1996; Liu and Nagel, 2001, and references therein). A model that combines frictional and kinetic theories was proposed by Savage (1998). The model includes a yield condition plus an associated flow rule and it accounts for fluctuations in the deformation rate tensor at any location about the mean value. The mean stress tensor is determined by averaging over the entire range of deformation, assuming that the strain rate fluctuations follow a Gaussian distribution. This assumption leads to Newtonian constitutive relations, with bulk and shear viscosities of the granular material that are not necessarily constant but are related to the structure of the granular material (Savage, 1998). There are many other studies on the liquid-like flow of dense granular material and there is no accepted view on this topic.

The experimental observations of Lube et al. (2004) demonstrate that during a flow with roughly constant-velocity, granular material exhibits common features to Newtonian fluid with effective viscosity representing frictional interactions between particles. During a period of lowering velocity, instead of gradual deceleration the granular flow comes to an abrupt halt. Jop et al. (2006) presented related theoretical and experimental results supporting the idea that a simple visco-plastic

approach can capture the main properties of granular flow and could serve as a basic tool for modeling more complex flows in geophysical or industrial applications. Following these ideas we approximate the rate of granular flow, or the rate of accumulation of the irreversible strain component, by Newtonian constitutive relation:

$$\frac{d\varepsilon_{ij}^{(p)}}{dt} = \tau_{ij} \cdot C_g \cdot B^n, \tag{18}$$

where C_g is the compliance or fluidity (inverse of viscosity) of the fine grain granular material ($B=1$) and n is a power index; $\tau_{ij} = \sigma_{ij} - (1/3)\sigma_{kk}\delta_{ij}$ is the deviatoric part of the stress tensor. With relatively high values of the power index, the Newtonian-like granular flow is realized only for breakage values $B \approx 1$ and ongoing loading ($\xi > \xi_0$) that support the increase of the breakage parameter B.

3. Numerical results

We present two different model solutions to illustrate several features of the formulated CDBM. We simulate first quasi-static evolution of damage in a sample subjected to uniaxial load under constant confining stress, and demonstrate the conditions for fragmentation or shear granular flow. The dynamics of the breakage growth is studied in a second case dealing with evolving deformation and material properties in a narrow zone subjected to constant compacting strain and increasing shear strain due to motion of outer elastic blocks.

3.1. Damage evolution under uniaxial loading

As mentioned, the accumulation of damage toward the critical value ($\alpha=\alpha_{cr}$) can lead to two different effective granular phases and modes of failure. Mode-II failure and transition to pseudo-liquid granular flow under compression occur within the interval of the strain invariants ratio $\xi_0 \le \xi \le \xi_1$. At higher values of the strain invariants ratio ($\xi_1 < \xi$) mode-I failure leads to pseudo-gas and fragmentation. Fig. 5 shows evolving damage along with change of the ξ-value in a sample with $\lambda_0=\mu_0=10^{10}$ Pa subjected to uniaxial load under constant confinements of $P_c=0$, 10 and 50 MPa. The first three cases are simulated for relatively strong material with $\xi_0=-0.8$ corresponding to high internal friction coefficient of about 0.83. With these material parameters, the transition between granular flow and fragmentation (for $\alpha=\alpha_{cr}$) occurs at $\xi_1=0.82$. The time scale in Fig. 5 is normalized to the time to failure under $P_c=10$ MPa. Each model run shown in Fig. 5 starts with 3-D compaction ($\xi=-\sqrt{3}$) and zero damage. With increasing load, the strain invariants ratio increases and when it reaches ξ_0 the damage α begins to increase with increasing rate toward α_{cr}.

For the unconfined case ($P_c=0$ MPa, blue line) the final ξ-value is only slightly above ξ_1 (Fig. 5 lower panel). However, even for small confining pressure ($P_c=10$ MPa, red line) the final ξ-value is below ξ_1. Further increase of the confinement ($P_c=50$ MPa, green line) decreases further the final ξ-value. These results only slightly depend on the Poisson ratio of the intact material (0.25 in the presented case), but they depend significantly on the material strength ξ_0. The violet line in Fig. 5 presents simulation results for material with $\xi_0=-0.9$ corresponding to lower internal friction coefficient of about 0.68 and lower $\xi_1=0.77$. In this case, under $P_c=10$ MPa confinement the final ξ-value is well above ξ_1. These examples demonstrate that the mode of failure strongly depends on the internal friction coefficient of the starting material. Relatively weak

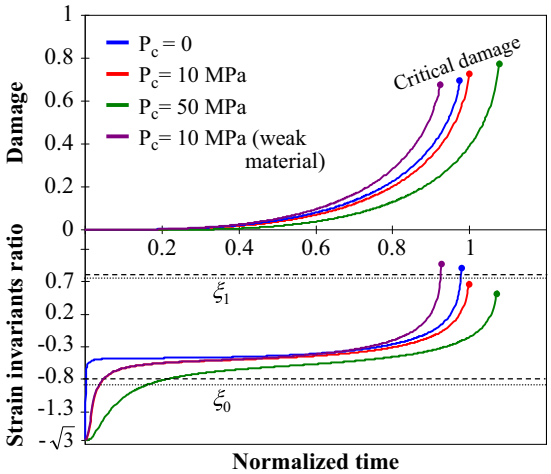

Fig. 5. Damage accumulation up to the critical value and related change of the strain invariants ratio in a sample subjected to uniaxial loading with constant confining pressure $P_c=0$, 10 and 50 MPa. The dashed lines define the onset of damage for strong material with $\xi_0=-0.8$ and transition between granular flow and fragmentation phases for $\xi_1=0.82$. The dotted lines define the onset of damage for weaker material with $\xi_0=-0.9$ and transition between granular flow and fragmentation phases for $\xi_1=0.77$.

materials may be fragmented not only for unconfined load but also with small confinement, while stronger materials under some confinement sustain at $\alpha=\alpha_{cr}$ a mode-II failure and transition to granular flow.

3.2. Damage and breakage evolution in a long narrow zone

Here we discuss a simplified model describing the transition from quasi-static damage evolution to fast breakage growth and dynamic slip event. The model geometry and set-up (Fig. 6) is similar to a case examined by Lyakhovsky et al. (2011). This setting is motivated by dynamic slip events in large earthquake faults that tend to occur within a highly localized damage zone with width of 10^{-3}–10^{-5} m (e.g., Chester et al., 1993; Heermance et al., 2003; Rockwell and Ben-Zion, 2007).

The material in the narrow zone is subjected to constant compaction, ε_c, and increasing shear strain due to motion of the bounding elastic blocks. The total shear strain, ε_t, of the damage zone is the sum of reversible elastic component, ε, and irreversible (viscous) component ε_v associated with granular flow with the onset of breakage. The total shear strain is equal to the displacement at the edge of the damage zone divided by its width:

$$\varepsilon_t=\varepsilon+\varepsilon_v=\frac{u(t)}{w}. \tag{19}$$

We define an irreversible (viscous) displacement component, $u_v=\varepsilon_v\cdot w$, and related irreversible strain rate $e=d\varepsilon_t/dt=1/w\cdot du(t)/dt$. With these notations, the elastic strain, its invariants, and ratio of the strain invariants are:

$$\begin{aligned}&\varepsilon=\frac{u(t)-u_v(t)}{w}\\&I_1=3\varepsilon_c\\&I_2=3\varepsilon_c^2+2\varepsilon^2\\&\xi=\frac{I_1}{\sqrt{I_2}}=\frac{3\varepsilon_c}{\sqrt{3\varepsilon_c^2+2\varepsilon^2}}.\end{aligned} \tag{20}$$

We use the conditions of convexity of the elastic strain energy (2), and the equation for critical damage derived by Lyakhovsky et al. (2011, Eq. 35), for a 1-D case with $\varepsilon_c=const$. Balancing the stresses at the interface between the elastic block and the narrow damage zone leads (see Lyakhovsky et al., 2011 for detailed derivations) to a final equation describing the evolution of the system:

$$\frac{\mu_0}{V_S}\frac{du}{dt}=\mu_0\cdot\frac{u_0-u}{L}-(2\cdot\mu(\alpha)-\gamma(\alpha)\cdot\xi)\cdot\frac{u-u_v}{w}. \tag{21}$$

The term on the left represents a planar shear wave radiated from the narrow zone and traveling in the outer elastic blocks with velocity V_S. This is usually referred to as radiation damping (e.g., Rice and Ben-Zion, 1996).

Eq. (21) coupled with Eqs. ((15), (16), (17)) for the damage and breakage evolution, and Eq. (18) for the rate of the granular flow, fully define the evolution of the system for given initial conditions and outer block velocity. These equations are solved numerically for different sets of model parameters given in Table 1. The numerical simulations are done for a

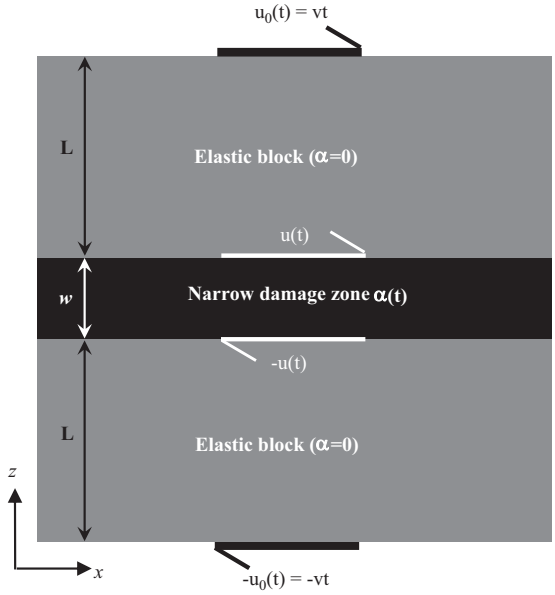

Fig. 6. Model configuration with a uniform narrow damage zone between two purely elastic blocks moving with constant velocity.

Table 1
Parameters of the model runs.

	C_d (s^{-1})	C_B (s^{-1})	β	C_g, $(Pa\ s)^{-1}$	n
1	10	100	0.005	10^{-5}	10
2	10	200	0.005	10^{-5}	10
3	10	300	0.005	10^{-5}	10
4	10	300	0.005	10^{-5}	5
5	10	300	0.005	10^{-5}	1
6	10	300	0.01	10^{-5}	10
7	10	300	0.02	10^{-5}	10

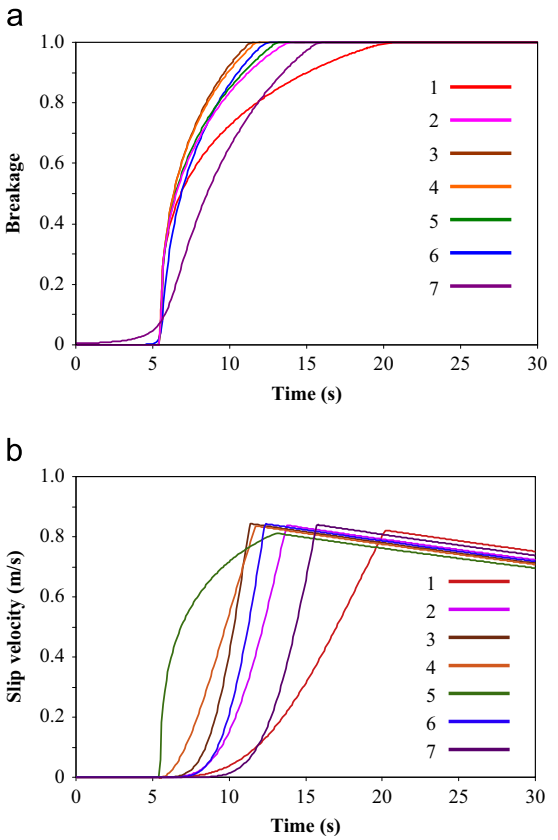

Fig. 7. Simulated breakage evolution (a) and slip rate (b) in the model shown in Fig. 6. Zero time ($t=0$) corresponds to about 5 s before the onset of breakage accumulation. The model parameters are given in Table 1.

model size of $L=10^4$ m which is several orders of magnitude larger than the damage zone width (10^{-3}–10^{-5} m). To increase the stability and efficiency of the simulations we use $w=10^{-3}$ m. Typical values for the elastic moduli of intact crystalline rocks are $\lambda_0 \sim \mu_0 \sim 10^{10}$ Pa. Characteristic values of the parameters controlling the onset of damage and its kinetics ($\xi_0=-0.8$, $C_d=10\ s^{-1}$) are constrained from previous laboratory studies (e.g., Hamiel et al., 2004; Lyakhovsky et al., 2005) and are kept the same for all model runs. Since these parameters control slow damage accumulation compared to the duration of the solid-granular transition, their values have almost negligible effect on the dynamics of the phase transition. The expected slip velocity v during seismic events is of the order of meter per second, and the estimated shear stress τ in the seismogenic zone of earthquake faults is of the order of 10–100 MPa (e.g., Ben-Zion, 2001). These values define the effective viscosity of the granular flow $\eta=\tau w/v$ (stress multiplied by width and divided by slip rate). For $w=10^{-3}$ m, $\tau=100$ MPa and $v=1$ m/s, the viscosity is 10^5 Pa s and corresponds to $C_g=10^{-5}$ /Pa s. The role of this parameter is straight forward and its value is kept constant for all runs. The roles of the parameters controlling the breakage accumulation, C_B, β, and power index n, are less obvious and demonstrated with results of numerical simulations using different parameter values.

The most important quantities characterizing the dynamics of the phase transition are the evolution of the breakage parameter and slip-rate. Fig. 7 shows simulations of these variables for various values of controlling parameters. The zero time ($t=0$) corresponds to about 5 s before the onset of breakage accumulation; the preceding long period of stress and damage accumulation is not shown. The first set of three model runs with different C_B values (see Table 1 for model

parameters) indicates that C_B is the most important parameter controlling the duration of the transition from $B=0$ to $B=1$ (Fig. 7a), as well as the rise time of the slip velocity (Fig. 7b). For $C_B=100\ s^{-1}$, which is 10 times the C_d value, the breakage growth takes about 15 s. As C_B increases the duration of the transition decreases proportionally. The breakage growth is only slightly affected by variations of the power index in the granular flow (runs 4 and 5) but the slip velocity changes significantly. With high power index ($n=10$) the slip rate increases rapidly to a peak value, and then start decreasing slowly after an initial sharp reduction at high breakage values. During the stage of fast breakage increase, the viscosity of the granular material decreases leading to slip rate acceleration. When the breakage approaches its maximal value ($B=1$), the viscosity remains constant and the slip rate starts to decrease according to Maxwell stress relaxation. This transition appears in Fig. 7b as kinks, since the rate of breakage accumulation is relatively high in the presented model runs. The transition between the acceleration and relaxation stages becomes smoother in models with low power index, like run ♯5 with $n=1$ (green line in Fig. 7), or slow breakage growth (not shown here).

The β parameter controls the onset and early stage of the breakage growth (runs 6 and 7). According to (17), significant breakage growth starts at lower damage values with larger β, and the early growth is more gradual. However, at the later stage following the peak slip rate, the shapes of both the breakage and slip rate curves are largely unaffected by the β value other than showing shifts in time. The simulation results indicate that different model parameters have different impact on the system evolution and generated signals. This suggests that the parameters could be independently calibrated using laboratory or seismological observations.

4. Discussion

We develop a theoretical model for continuum damage–breakage mechanics (CDBM) and use the model to examine basic aspects of a phase transition at a critical level of material damage from solid to granular material. The model combines and extends previous results of a continuum damage model that accounts for distributed cracks by adding to the energy function an additional nonlinear term and using a scalar damage parameter α (Lyakhovsky et al., 1997, 2011), and a continuum breakage model that measures the relative distance of a given grain size distribution of a granular phase from the initial to the ultimate distribution with a breakage parameter B (Einav, 2007a, b). The developed CDBM provides a framework that can be used to analyze the progression of deformation from a stable distributed brittle cracking in a solid with evolving elastic moduli, to localization of deformation and dynamic rupture in a zone with granular material having one or more vanishing elastic moduli.

The model predicts that damage accumulation toward its critical value can lead to two different modes of failure involving a transition in the state and behavior of the material: a pseudo-liquid granular flow or a pseudo-gas fragmentation. These different modes depend on the strain invariants ratio value ξ_1 (7) at the critical damage level, and they correspond to axial-splitting/fragmentation or shear localization and rupture observed in laboratory experiments. Shear failure occurs within the interval of the strain invariants ratio $\xi_0 \le \xi \le \xi_1$, while axial-splitting and fragmentation is expected at higher values involving little to no confinement ($\xi > \xi_1$). Numerical simulations demonstrate that the transition between these modes of failure depends on the internal friction coefficient of the intact material. With small confinement, strong samples subjected to uniaxial load are expected to fail by shear while weak materials can fail by axial splitting. Increasing confinement suppresses the pseudo-gas fragmentation mode. The simulation results also predict that the failure mode should depend on the micro-structure and grain size of the starting material through its internal friction coefficient. Such effects were reported in several studies with cementation materials, finding that pure cement samples usually fail by splitting whereas concretes fail by shear (e.g., Santiago and Hildsorf, 1973; Swami and Kameswara, 1973; Dyskin et al., 1996).

The dynamics of the transition from solid to pseudo-liquid phase, associated with the breakage growth, is examined by modeling deformation and evolution of material properties in a narrow zone subjected to constant compacting strain and increasing shear strain. The model results exhibit (Fig. 7) a transition from early quasi-static damage evolution to fast breakage growth and dynamic slip event. This is analogous to transitions from stable to unstable slip in frictional and plasticity models (e.g., Rice, 1980), although our model is more general in that it accounts also for the evolution of material properties with deformation. The simulation runs demonstrate that different model parameters have different impact on the duration of the transition to dynamic slip and the shapes of the breakage growth and slip rate curves, offering possibilities for constraining the model parameters.

Following failure and reduction of the loading below the yielding threshold $\xi=\xi_0$, the damage model predicts material healing (Lyakhovsky et al., 1997, 2005) associated with recovery of the elastic moduli of the solid phase. The damage healing is consistent with the presented thermodynamic formulation since the derivative $\partial F/\partial\alpha$ (Eq. (13)) changes its sign. Based on the results discussed so far, once the solid-granular transition occurs the energy of the granular phase with $B=1$ remains below the energy of the solid phase. This energy difference would prevent the reversed transition from the granular to the solid phase, even under compressive stresses without any differential load. This limitation might be overcome by further refinement of the energy function. The classical thermodynamic theory of phase transition always incorporates certain modifications of the basic energy function, such as the Van der Waals equation of state. The theory for second-order phase transitions of Landau is based on a phenomenological expression for the free energy as a 4th order polynomial function of the order parameter. Below we discuss a possible route for constructing a modified energy of the granular phase that can be used to study a granular-solid transition associated with post-failure healing.

Hamiel et al. (2011) represented the general form of the elastic energy function with two strain invariants as:

$$F(I_1,\ I_2) = I_2 \cdot f(\xi), \tag{22}$$

where $f(\xi)$ is some function. This provides an explicit representation of a general second-order strain energy function. The elastic potential (2) can be obtained from (22) by using a polynomial function $f(\bullet)$ up to the second order:

$$f(\xi) = a_0 + a_1\xi + a_2\xi^2. \tag{23}$$

Substituting (23) back into (22) leads to

$$F(\varepsilon_{ij}) = a_0 I_2 + a_1 I_1\sqrt{I_2} + a_2 I_1^2, \tag{24}$$

which differs from (2) only in the notation of the coefficients. These results show that the functional form (2) is equivalent to a Taylor expansion up to the second order of the function $f(\bullet)$ in (22). We suggest that the following higher-order expansion of $f(\bullet)$ should be adopted for the granular phase energy F_B instead of (9):

$$f(\xi) = a_0 + a_1\xi + a_2\xi^2 + a_3\xi^3. \tag{25}$$

Substituting (25) back into (22) leads to

$$F_B(\varepsilon_{ij}) = a_0 I_2 + a_1 I_1\sqrt{I_2} + a_2 I_1^2 + a_3\frac{I_1^3}{\sqrt{I_2}}, \tag{26}$$

Taking the derivative of the energy form (26) with respect to the strain leads to the following stress-strain relation:

$$\sigma_{ij} = (2a_2 + a_1/\xi + 3a_3\xi)I_1\delta_{ij} + (2a_0 + a_1\xi - a_3\xi^3)\varepsilon_{ij}. \tag{27}$$

Eqs. (26, 27) show that the third order term with a_3 may be important only for conditions near 3-D compaction or 3-D tension ($\xi \to \pm\sqrt{3}$), and is not expected to affect the stress-strain curve under relatively large differential load. Therefore, this term was ignored by Hamiel et al. (2011) and the developments of this work. However, the modified F_B (26) provides thermodynamically consistent conditions for breakage decrease (healing) under 3-D compaction.

Fig. 8 shows the normalized energy F_S/I_2 of the solid phase (black line from Fig. 2), the granular phase (F_B/I_2, red line with θ=0.7 from Fig. 2), and the modified energy (26). The values of the coefficients a_0 to a_3 were chosen to meet the following conditions: vanishing of both effective elastic moduli in (27) for $\xi=\xi_1$, and crossing the solid phase energy at a given ξ value ($F_S=F_B$ for $\xi=\xi_d$). The modified granular phase energy (blue line in Fig. 8) is almost identical to the energy defined in (9) for positive ξ values, but it starts to deviate at negative values ($\xi\sim-0.2$ marked by dotted line). The cubic ξ-term in (26) leads to a relatively steep increase of the modified F_B when approaching 3-D compaction. The blue line for the modified energy (26) crosses the black line for the solid phase energy, and $F_B > F_S$ for $\xi < \xi_d$ producing breakage decrease toward the less energetic solid phase. The modified energy for the granular phase (26) allows thermodynamically consistent transitions between the two phases in both directions: from solid to granular under high differential load and from granular to solid phase under compaction. Relatively fast breakage decrease, together with high power index n in the Eq. (18) for the rate of granular flow, can lead to rapid viscosity increase. This should stop the

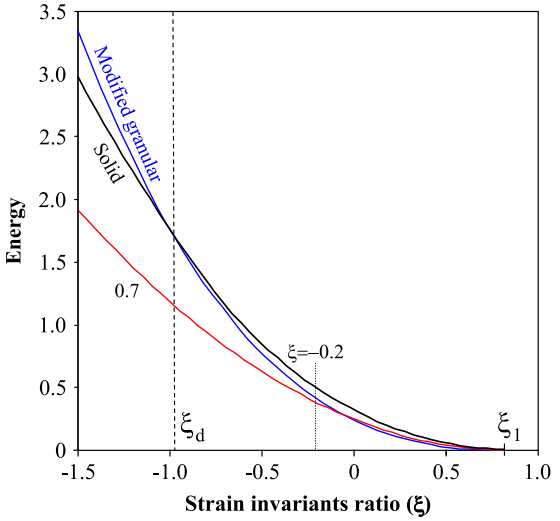

Fig. 8. Normalized energy (F_S/I_2, $\lambda_0=\mu_0=1$) of the solid phase (black line) and the granular phase (F_B/I_2) for θ=0.7 (red lines) within extended interval below ξ_0 value where the reversed transition from granular pseudo-liquid phase to solid is expected. The modified granular phase energy (blue line) is almost identical to the energy defined in (9) for positive ξ values, but begins to deviate at negative values ($\xi\sim-0.2$) and crosses the black line at $\xi=\xi_d$. (For interpretation of the references to color in this figure legend, the reader is referred to the web version of this article.)

motion of the granular flow, similarly to the behavior of classical visco-plastic fluids such as Bingham fluid, and be followed by a transition to a (damaged) solid phase.

In conclusion, we introduced a novel approach to analyze the problem of brittle instability by combining continuum damage and continuum breakage models in a thermodynamically-consistent formulation. The macroscopic instability of the solid phase is associated with a phase transition in a localized zone having a pseudo-liquid or pseudo-gas phase. Eq. (26) for the modified energy of the granular phase may be used to analyze the reversed granular-solid transition. This will be done in a subsequent study.

Acknowledgments

We acknowledge support by the US–Israel Binational Science Foundation (grant 2008248) and the National Science Foundation (grant EAR-0908903). The manuscript benefitted from useful comments by two anonymous referees.

Appendix A. Thermodynamic formulation

The total energy of a solid with a unit mass includes internal and kinetic components:

$$E = E_k + U. \tag{A1}$$

The specific kinetic energy of the solid is $E_k = v_i v_i/2$ with v_i being velocity and the internal energy is expressed through the free energy F, temperature T and entropy S as $U=F+TS$. The energy balance equation dictates that the change in the energy of a system is equal to the divergence of the heat flux $J_i^{(q)}$ and total external work W

$$\frac{dE}{dt} = \frac{dE_k}{dt} + \frac{d}{dt}(F+TS) = -\nabla_i J_i^{(q)} + W. \tag{A2}$$

The entropy balance equation includes entropy flux $J_i^{(s)}$ and non-negative local entropy production Γ

$$\frac{dS}{dt} = -\nabla_i J_i^{(s)} + \Gamma, \quad \Gamma \geq 0. \tag{A3}$$

The non-negative local entropy production results from all the dissipative irreversible processes in the medium including internal friction and damage evolution. From Eq. (1) of the main text, the change in the free energy can be expressed as

$$dF = -SdT + \frac{\partial F}{\partial \varepsilon_{ij}} d\varepsilon_{ij} + \frac{\partial F}{\partial \alpha} d\alpha + \frac{\partial F}{\partial B} dB. \tag{A4}$$

The local entropy production may be represented as:

$$\Gamma - \nabla_i \left(J_i^{(s)} - \frac{J_i^{(q)}}{T} \right) = \Gamma_M + \Gamma_H + \Gamma_{DB}. \tag{A5}$$

The terms on the right side of (A5) are associated with the following energy components: mechanical work

$$\Gamma_M = -\frac{1}{T}\left[v_i \frac{dv_i}{dt} + \frac{\partial F}{\partial \varepsilon_{ij}} e_{ij} - W \right], \tag{A6}$$

heat transport

$$\Gamma_H = -\frac{1}{T^2} J_i^{(q)} \nabla_i T, \tag{A7}$$

and damage–breakage evolution

$$\Gamma_{DB} = -\frac{1}{T}\left(\frac{\partial F}{\partial \alpha} \frac{d\alpha}{dt} + \frac{\partial F}{\partial B} \frac{dB}{dt} \right). \tag{A8}$$

Following the literature of non-equilibrium thermodynamic (e.g., deGroot and Mazur, 1962), the divergence term on the left side of (A5) is eliminated by defining the entropy flux as

$$J_i^{(s)} = \frac{J_i^{(q)}}{T}. \tag{A9}$$

The equation of motion of a continuum is given by the standard relation

$$\rho \frac{dv_i}{dt} = \frac{\partial \sigma_{ij}}{\partial x_j} + f_i, \tag{A10}$$

where f_i is the body force. The model formulation should satisfy conservation of mechanical energy ($\Gamma_M=0$) if all the dissipative processes in the system are frozen. This condition leads to the definition of the stress tensor

$$\sigma_{ij}=\rho\frac{\partial F}{\partial \varepsilon_{ij}}. \tag{A11}$$

The energy form (1) of the main text may be extended by additional gradient type non-local terms associated with $\nabla\alpha$, as in the CDM of Lyakhovsky et al. (2011). In this case, the entropy fluxes Γ_M and Γ_{DB} will include additional terms leading to "structural stresses" in the constitutive relations (A11) and damage-diffusion in the equations for the damage evolution. Detailed derivations of such terms may be found in Lyakhovsky et al. (2011).

References

Agnon, A., Lyakhovsky, V., 1995. Damage distribution and localization during dyke intrusion. In: Baer, G., Heimann, A. (Eds.), The Physics and Chemistry of Dykes. Balkema, Rotterdam, pp. 65–78.

Allix, O., Hild, F., 2002. Continuum damage mechanics of materials and structures. Elsevier396.

Ben-Zion, Y., 2001. Dynamic rupture in recent models of earthquake faults. J. Mech. Phys. Solids 49, 2209–2244.

Ben-Zion, Y., 2008. Collective behavior of earthquakes and faults: continuum-discrete transitions, evolutionary changes and corresponding dynamic regimes. Rev. Geophys. 46, RG4006, http://dx.doi.org/10.1029/2008RG000260.

Ben-Zion, Y., Dahmen, K.A., Uhl, J.T., 2011. A unifying phase diagram for the dynamics of sheared solids and granular materials. Pure Appl. Geophys. 168, 2221–2237, http://dx.doi.org/10.1007/s00024-011-0273-7.

Ben-Zion, Y., Sammis, C.G., 2003. Characterization of fault zones. Pure Appl. Geophys. 160, 677–715.

Bhat, H.S., Sammis, C.G., Rosakis, A.J., 2011. The micromechanics of westerley granite at large compressive loads. Pure Appl. Geophys. 168 (12), 1–18, http://dx.doi.org/10.1007/s00024-011-0271-9.

Broberg, K.B., 1999. Cracks and Fracture. Academic Press, San Diego.

Byerlee, J.D., 1978. Friction of rocks. Pure Appl. Geophys. 116, 615–626.

Chester, F.M., Evans, J.P., Biegel, R.L., 1993. Internal structure and weakening mechanisms of the San Andreas fault. J. Geophys. Res. 98, 771–786.

deGroot, S.R., Mazur, P., 1962. Nonequilibrium Thermodynamics. North-Holland Publishing Co., Amsterdam.

Dyskin, A.V., Sahouryeh, E. and Ustinov, K.B. 1996. The role of micro-plasticity in the mechanisms of shear fracture and splitting in uniaxial compression. In: Aubertin M., Hassani F., Mitri H. (Eds.). Proceedings of the Second North American Rock Mechanics Symposium. Rock Mechanics Tools and Techniques,, vol. 2, pp. 1611–1618.

Einav, I., 2007a. Breakage mechanics – Part I: theory. J. Mech. Phys. Solids 55, 1274–1297.

Einav, I., 2007b. Breakage mechanics – Part II: modeling granular materials. J. Mech. Phys. Solids 55, 1298–1320.

Ekeland, I., Temam, R., 1976. Convex analysis and variational problems. Elsevier, Amsterdam.

Ericksen, J.L., 1998. Introduction to the Thermodynamics of Solids. Springer-Verlag, NY.

Hamiel, Y., Liu, Y., Lyakhovsky, V., Ben-Zion, Y., Lockner, D., 2004. A visco-elastic damage model with applications to stable and unstable fracturing. J. Geophys. Int. 159, 1155–1165.

Hamiel, Y., Lyakhovsky, V., Stanchits, S., Dresen, G., Ben-Zion, Y., 2009. Brittle deformation and damage-induced seismic wave anisotropy in rocks. Geophys. J. Int. 178, 901–909, http://dx.doi.org/10.1111/j.1365-246X.2009.04200.x.

Heermance, R., Shipton, Z.K., Evans, J.P., 2003. Fault structure control on fault slip and ground motion during the 1999 rupture of the Chelungpu fault, Taiwan. Bull. Seis. Soc. Am. 93, 1034–1050.

Jaeger, J.C., Cook, N.G.W., 1979. Fundamentals of rock mechanics. Chapman and Hall, London.

Jaeger, H.M., Nagel, S.R., Behringer, R.P., 1996. Granular Solids, Liquids, and Gases. Rev. Mod. Phys. 68, 1259–1273.

Jop, P., Forterre, Y., Pouliquen, O., 2006. A constitutive law for dense granular flows. Nature 441, 727–730, http://dx.doi.org/10.1038/nature04801.

Kachanov, L.M., 1986. Introduction to continuum damage mechanics. Martinus Nijhoff Publishers, Dordrecht, The Netherland.

Karrech, A., Duhamel, D., Bonnet, G., Roux, J.N., Chevoir, F., Canou, J., Dupla, J.C., Sab, K., 2007. A computational procedure for the prediction of settlement in granular materials under cyclic loading. Comput. Methods Appl. Mech. Engrg 197, 80–94.

Krajcinovic, D., 1996. Damage Mechanics. Elsevier, Amsterdam.

Lemaitre, J., 1996. A Course on Damage Mechanics. Springer Verlag, Berlin228.

Liu, A.J., Nagel, S.R. (Eds.), 2001. Jamming and Rheology: Constrained Dynamics on Microscopic and Macroscopic Scales. Taylor and Francis, London.

Lockner, D.A., Byerlee, J.D., Kuksenko, V., Ponomarev, A., Sidorin, A., 1992. Observations of quasi-static fault growth from acoustic emissions. In: Evans, B., Wong, T.-F. (Eds.), Fault mechanics and transport properties of rocks, International Geophysics Series, vol. 51. . Academic Press, San Diego, CA, pp. 3–31.

Lube, G., Huppert, H.E., Sparks, R.S.J., Hallworth, M.A., 2004. Axisymmetric collapses of granular columns. J. Fluid Mech. 508, 175–199.

Lyakhovsky, V., Ben-Zion, Y., Agnon, A., 1997. Distributed damage, faulting, and friction. J. Geophys. Res. 102, 27635–27649.

Lyakhovsky, V., Ben-Zion, Y., Agnon, A., 2005. A viscoelastic damage rheology and rate- and state-dependent friction. Geophys. J. Int. 161, 179–190.

Lyakhovsky, V., Hamiel, Y., Ben-Zion, Y., 2011. A non-local visco-elastic damage model and dynamic fracturing. J. Mech. Phys. Solids 59, 1752–1776, http://dx.doi.org/10.1016/j.jmps.2011.05.016.

Malvern, L.E., 1969. Introduction to the mechanics of a continuum medium. Prentice-Hall, Inc., New Jersey.

Myasnikov, V.P., Oleinikov, A.I., 1991. Deformation model of a perfectly free-flowing granular medium. Sov. Phys. Dokl. 36, 51–53.

Nguyen, V.-H., Duhamel, D., Nedjar, B., 2003. A continuum model for granular materials taking into account the no-tension effect. Mech. Mater. 35, 955–967.

Onsager, L., 1931. Reciprocal relations in irreversible processes. Phys. Rev. 37, 405–416.

Perrin, G., Leblond, J.B., 1993. Rudnicki and Rice's analysis of strain localization revisited. J. Appl. Mech. 60, 842–846.

Rabotnov, Y.N. 1988. Mechanics of deformable solids, Science, Moscow, pp. 712.

Rice, J.R., 1980. The mechanics of earthquake rupture. In: Dziewonski, A.M., Boschi, E. (Eds.), Physics of the Earth's Interior. Italian Physical Society/North Holland, Amsterdam, pp. 555–649.

Rice, J.R., 1993. Spatio-temporal complexity of slip on a fault. J. Geophys. Res. 98, 9885–9907.

Rice, J.R., Ben-Zion, Y., 1996. Slip complexity in earthquake fault models. Proc. Natl. Acad. Sci. USA 93, 3811–3818.

Rockwell, T.K., Ben-Zion, Y., 2007. High localization of primary slip zones in large earthquakes from paleoseismic trenches: observations and implications for earthquake physics. J. Geophys. Res. 112, B10304, http://dx.doi.org/10.1029/2006JB004764.

Rudnicki, J.W., Rice, J.R., 1975. Conditions for localization of deformation in pressure-sensitive dilatant materials. J. Mech. Phys. Solids 23, 371–394.

Santiago, S.D., Hildsorf, H., 1973. Fracture mechanisms of concrete under compressive loads. Cement and Concrete Research 3, 363–388.

Savage, S.B., 1998. Analyses of slow high-concentration flows of granular materials. J. Fluid Mech. 377, 1–26.

Stanchits, S., Vinciguerra, S., Dresen, G., 2006. Ultrasonic velocities, acoustic emission characteristics and crack damage of basalt and granite. Pure Appl. Geophys. 163, 974–993, http://dx.doi.org/10.1007/s00024-006-0059-5.

Swami, R.N., Kameswara, C.V.S., 1973. Fracture mechanism in concrete systems under uniaxial loading. Cem. Concr. Res. 3, 413–427.